Supporting Information

Nanopatterning of a stimuli-responsive fluorescent supramolecular polymer by thermal scanning probe lithography

Samuel Tobias Zimmermann,[†,∥] *Diederik Wilhelmus Rienszen Balkenende,*[‡,§,∥] *Anna Lavrenova,*[‡] *Christoph Weder,**[‡] *Jürgen Brugger.**[†]

[†]Microsystems Laboratory, École Polytechnique Fédérale de Lausanne, CH-1015, Lausanne, Switzerland

[‡]Adolphe Merkle Institute, University of Fribourg, 1700 Fribourg, Switzerland

Diffusion-limited aggregation of OPV

In previous studies on blends of small amounts (1-2% w/w) of cyano-OPV derivatives in glassy host polymers [1–3], it was possible to quench bulk samples of the materials with the cyano-OPVs kinetically trapped in the green-light-emitting monomeric (disassembled) state, by rapidly cooling the blends from the homogeneous melt to below the glass transition temperature (where the dye molecules should aggregate on thermodynamic grounds). By contrast, it was so far not possible to achieve such behavior with UPy-OPV-UPy, i.e., quench the green-light-emitting melt into a green-light emitting solid[4] instead, orange-red emitting assemblies in which the OPV-

moieties aggregate to display excimer emission were always formed. It stands to reason that the aggregation process is ultimately diffusion limited and the fast aggregation of UPy-OPV-UPy is associated with a) the low melt viscosity of the latter (in fact the melt consists of depolymerized supramolecular monomer) and b) the much higher concentration of the OPV motif in UPy-OPV-UPy than in the aforementioned blends. While it was so far not possible to overcome OPV aggregation in bulk samples of UPy-OPV-UPy, arguably on account of slow heat dissipation and supramolecular polymer formation, the present experiments show clearly that the green-light emitting monomer state can be trapped if nanoscale voxels are heated by t-SPL. Indeed, when rapid indentation with a hot AFM probe occurs, the material around the tip-sample contact area is heated above the glass transition temperature and quenched rapidly after tip removal, due to the fast heat dissipation into the remainder of the sample.

Indentation force calibration of electrostatically actuated cantilevers

Currently in our commercial t-SPL tool, the indentation force is steered by setting a voltage for the electric potential between cantilever and substrate, which actuates the tip towards the sample. In order to convert the potential into an indentation force, the cantilever must be calibrated.[5] We use therefore a procedure similar to the one in Ref 5 which is described in the following section. As an approximation, the electrostatic force, which causes the cantilever to bend towards the substrate, is proportional to the square of the applied potential $F_{el} \propto V^2$. The deflection Δz of the cantilever induces a restoring force according to Hook's law $F_k = k_{spring} * \Delta z$ with k_{spring} being the spring constant of the cantilever. For the type of cantilevers used in this work, the spring constant is typically 0.9 nN/nm and is assumed to be linear for deflections in the range from 50 to 450 nm. When the cantilever is pulled towards the substrate without touching it, at the maximum deflection F_{el} and F_k are equal in accordance to Newton's law and therefore $\Delta z = k_{spring}^{-1} * F_{el}$. However due to the complex shape of the tip, the electrostatic force cannot *a priori* be calculated. In addition, the cantilever bending is affected by temperature gradients within the cantilever during thermal patterning, which is proportional to the heater temperature $\Delta z \propto T^2$. As a consequence, the deflection of the cantilever must be experimentally determined for different forces and temperatures and fitted to a model in order to compute the indentation force. For the calibration procedure, the tip was positioned at a vertical distance of 450 nm from the substrate and heated while an electrostatic potential of 2V between cantilever and substrate was applied. As a substrate, a silicon chip coated with poly-phthalaldehyde, a temperature sensitive resist which volatizes via self-amplified decomposition when heated above the degradation temperature was utilized.[6,7] The polymer serves as a detector due to its fast degradation (<2 µs)[7] and low degradation temperature (150-200 °C) to determine when the tip touches the substrate and

consequently creates an indent. If no indent was detected by scanning the surface in AFM mode, the procedure was repeated and the electrostatic potential was further increased in steps of 0.3 V until an indent was formed or until the electrostatic voltage exceeded 8 V without indent formation. In further iterations, the tip-sample distance was decreased down to 50 nm in steps of 20 nm and the voltage at which an indent was formed was recorded which resulted in a curve descrbing the bending of the cantilever as a function of the voltage. Multiple curves were recorded at different temperatures in order to extrapolate the cantilevers deflection caused by the heating as shown in Figure S1a. By using a numerical optimization package (*scipy*), the data points were then fitted with the model below.

$$\Delta z = f_V(V - f_{VOffs})^2 + f_T(T - T_{RT})^2$$

The parameters for the model which describe the measurements are $f_V = 7.80 \pm 0.6\, nmV^{-2}$, $f_{VOffs} = 0.8 \pm 0.3\, V$ and $f_T = 2.0 \cdot 10^{-4} \pm 1 \cdot 10^{-5}\, nmK^{-2}$ with a corresponding $R^2 = 0.97$. The square markers in Figure S1a correspond to the measured values and the solid lines correspond to the fitted model. The patterning force was then determined as the difference between the electrostatic force and the restoring force $F_{pat} = F_{el} - F_k = k\Delta z - kz_{piezo}$ where z_{piezo} was 200 nm for all experiments performed. Figure S1b shows the patterning force as a function of the electric potential for different temperatures, whereby a negative patterning force means that the deflection is not large enough to touch the substrate. We note that the method mentioned here neglects effects such as the interaction of the tip with the substrate while in contact and that not all tips have the same spring constant due to variations in geometry which occur naturally in the fabrication process. Nevertheless, the model represents the order of

magnitude of the governing forces and displays the relation between indentation force, electric tip actuation potential and heater temperature.

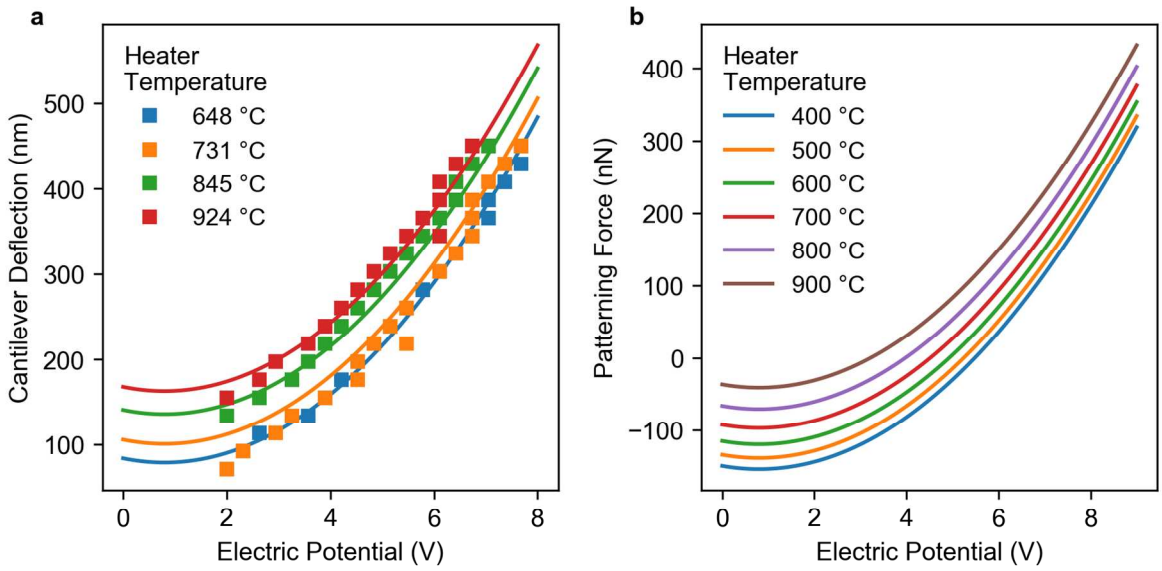

Figure S1. (a) Plot of the cantilever deflection as a function of the electrostatic potential between tip and substrate for different dip temperatures and the corresponding fitted curve (not all curves plotted for better visibility) (b) Plot of the computed patterning force as a function of the electric potential for different temperatures. A negative patterning force means that the tip is not in contact with the substrate

Evaluation of indents formed by t-SPL to determine the threshold temperature

The threshold temperature at which a material change can be detected by AFM upon indentation with the heated probe was determined by performing a series of indents at different indentation forces and heater temperatures as shown in Figure S2a. The recorded AFM topographies of the indents were then analyzed using a software script which extracts the maximum height and depth from each of the 16 indents as displayed in Figure S2b and computes the average value and standard deviation of the corresponding quantities.

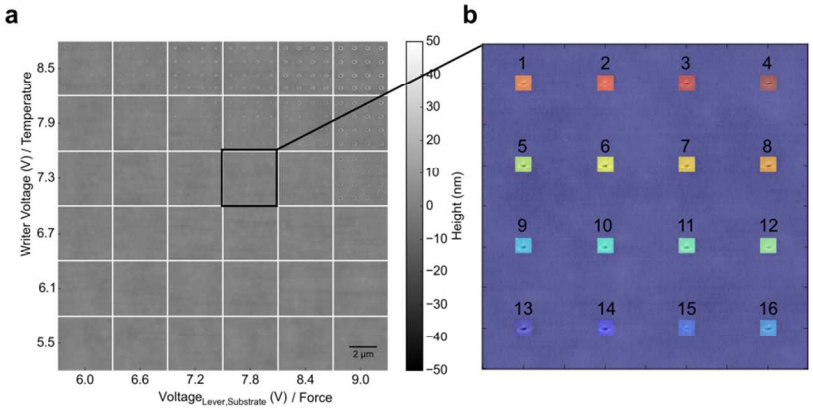

Figure S2. (a) Collection of 36 topography images obtained from t-SPL patterning at 6 different tip temperatures (writer voltage: 5.5 to 8.5 V) and indentation forces (voltage between cantilever and substrate: 6.0 to 9.0 V) (b) Magnification of one topography image with 16 labelled indents.

Thermal patterning and localizing of the fluorescent structures

Figure S3 shows how t-SPL patterns were labelled to identify them later in the fluorescence microscope. First, the t-SPL pattern of interest was written and in a second step, a number was added next to the pattern (Figure S3a), which allowed unambiguous identification of every pattern (Figure S3b).

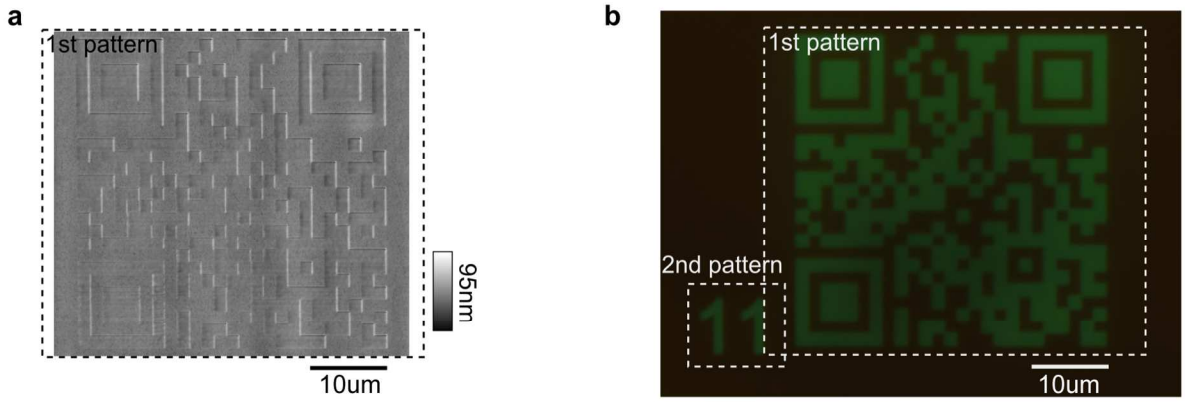

Figure S3. Thermal patterning and localization of the fluorescent structures. (a) AFM image of the thermal scanning probe pattern written into UPy-OPV-UPy. (b) Fluorescence image of the pattern of interest (1st pattern) and a second numeric pattern for identification. Frames show the scanned area with the t-SPL tool.

Relation between the pitch size and the pattern quality

Thermal patterning of polymers with a hot probe is challenging due to softening of the polymer and consecutive adhesion of viscous melt to the tip. For poly-phthalaldehyde, a self-amplified decomposing polymer this is not an issue since it decomposes at temperatures below the glass transition temperature (T_g).[6,7] In contrast, UPy-OPV-UPy becomes a viscous liquid above *T*g. We found that the pitch size is crucial, in order to obtain reproducible patterns. Figure S4 shows AFM topographies of patterns that have been fabricated with pitches ranging from 20 to 100 nm. One can observe in Figure S4a that at a pitch size of 20 nm material is displaced in the fast scan direction from left to right. The trench at the left, the irregular surface and the pile-up at the left side indicate that the tip displaces material in the fast scan direction. The pile-up decreases with increasing pitch size until 80 nm where the individual indents are visible as shown in Figure S4b. It is hypothesized, that the displacement is due to the consecutive displacement of material formed around an indent in fast scan direction by a distance that is approximately on the range of the tip apex diameter, which results in a net displacement of material over the entire pattern. On the contrary, if the pitch size is larger than the tip apex diameter the pile-up remains around the indent as sketched in Figure S4c.

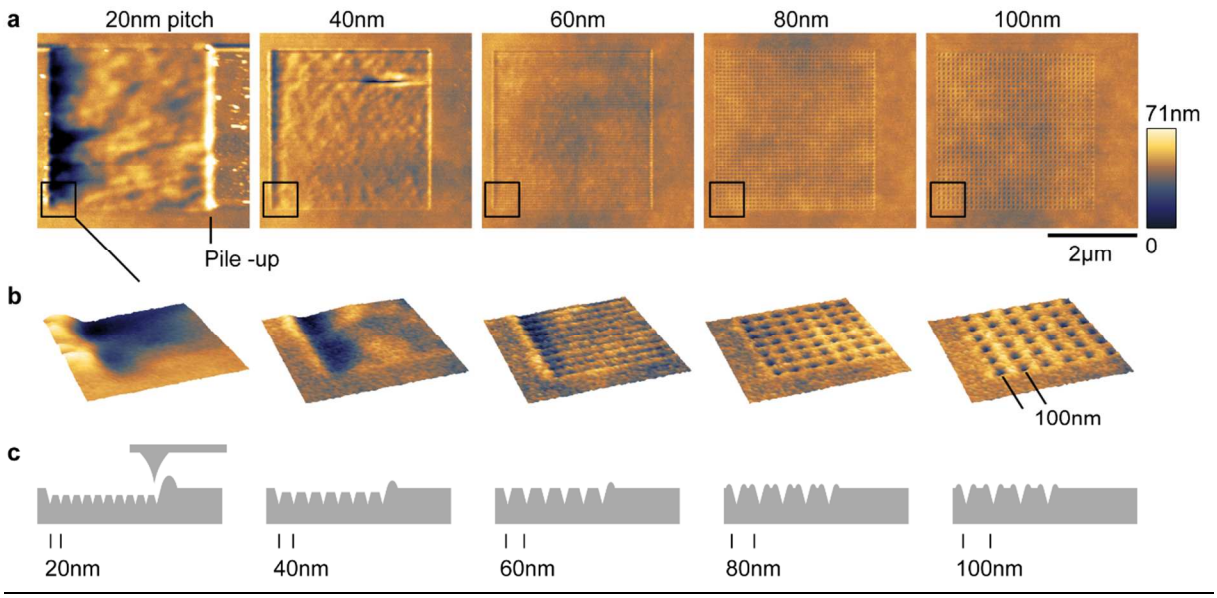

Figure S4. Influence of the indent distance on the quality of patterns. (a) AFM topography images of squares written by t-SPL into the UPy-OPV-UPy resist, using indent distances between 20 and 100 nm. (b) Magnified 3D topography images reveal the transition from plowing with the tip towards visibility of individual indents by increasing the spacing between individual indentations. (c) Schematic representation of the thermal indentation process and the influence of the indent distance on the topography.

Relation between pitch size and fluorescence intensity

To model the fluorescence intensity as a function of the pitch size, we assume that the thermally modified area has the shape of a semi-ellipsoid. This assumption is justified by the elliptic shape of the indents measured from the AFM topography (Figure 4c). The intensity per unit volume can be modelled as the ratio between a semi-ellipsoid's volume and the volume of the unit cell as depicted in Figure S5a. As long as the half pitch size L/2 is larger than the principle semi-axis a, the intensity and is inverse proportional to the square of the pitch size.

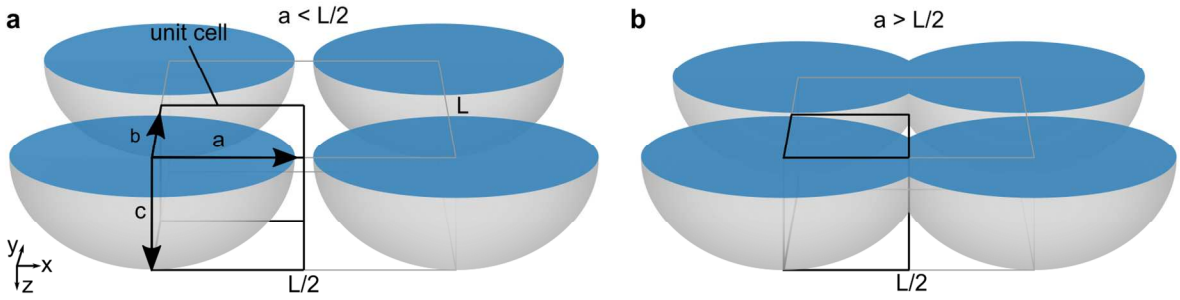

Figure S5. Unit cells with ellipsoidal indents as a model for the fluorescence intensity observed by optical fluorescence microscopy for (a) a half-pitch size larger than the principal semi-axis and (b) a half-pitch size smaller than the largest principle semi-axis.

As soon as the half-pitch is smaller than the major axis, the ellipsoids start to overlap as visualized in Figure S5b. As a consequence, the overlapping volume does not contribute to further increasing the fluorescence intensity. In the limit of the pitch size approaching zero, the whole unit cell is filled and the normalized intensity is one. The following function models the normalized fluorescence intensity as a function of the pitch size, and indent shape:

$$I(L,a,b) = \frac{V_{ellipsoid}(L,a,b,c)/8}{c*(L/2)^2} = \frac{4}{L^2}\cdot \int_0^{\min\left(\frac{L}{2},a\right)} \int_0^{\min\left(\frac{L}{2},\sqrt{1-(x/a)^2}\right)} \sqrt{1-\left(\frac{x}{a}\right)^2-\left(\frac{y}{b}\right)^2}\, dydx,$$

where a, b and c are the length of the principle semi-axes. We note here, that the normalized intensity, is independent of the indent depth c. To numerically evaluate the integral and fit the fluorescence intensity, a numerical optimization package *scipy* was used.

Proof-of-concept thermal patterning of fluorescent UPy-OPV-UPy

To acquire the fluorescence images shown in the manuscript, a short-pass filter was used to block the red background fluorescence from the unmodified supramolecular UPy-OPV-UPy glass. This was necessary to obtain a sufficiently strong contrast between the background and the modified area. To demonstrate the actual transition from red to green fluorescence, Figure S6a and b show a t-SPL pattern and the corresponding unfiltered image, respectively.

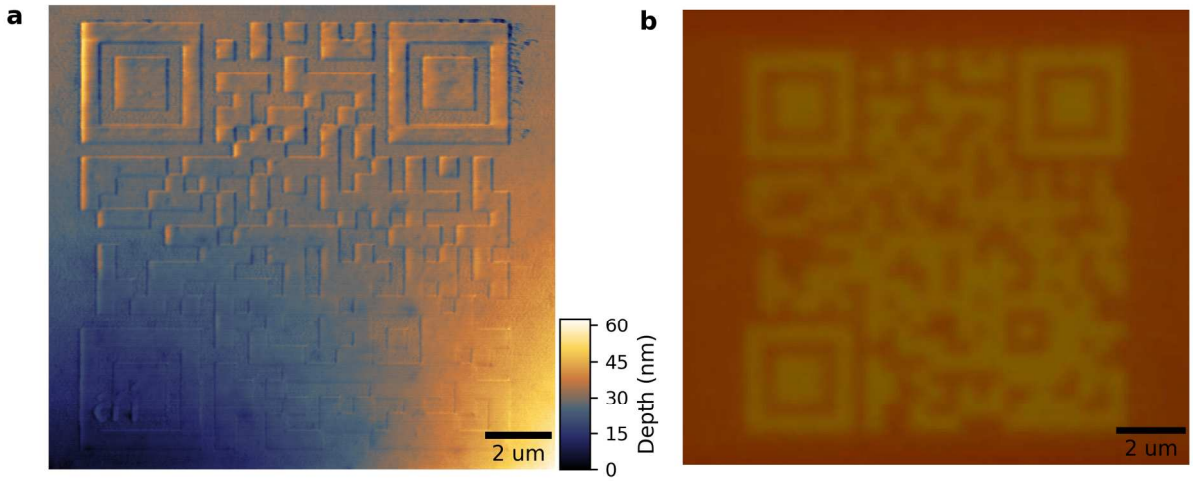

Figure S6. Proof-of-concept thermal patterning of a fluorescent structure. (a) AFM image after thermal patterning a QR code into the polymer. (b) Corresponding fluorescence image shows a clear contrast between modified (green fluorescent) and pristine (red fluorescent) substrate.

Hidden patterns visible with dark field microscopy due to deep indentation

Figure S7a shows a surface topography composed of two t-SPL patterns; a first square that has been completely exposed to heat and second the logos of “AMI” and “EPFL”. The concept to write a smaller pattern with the thermal probe within a larger pattern enables one to hide information from optical microscopy which can only be read out by sub nanometer precise methods such as atomic force microscopy. In Figure S7b, the fluorescence image of the two level structure does hide the second layer. However, when the features that are supposed to be hidden are too deep, dark field microscopy reveals the information even though they are virtually not visible by fluorescence microscopy (Figure S7c). As a consequence, the patterning depth of the second hidden layer should not exceed a few tens of a nanometer.

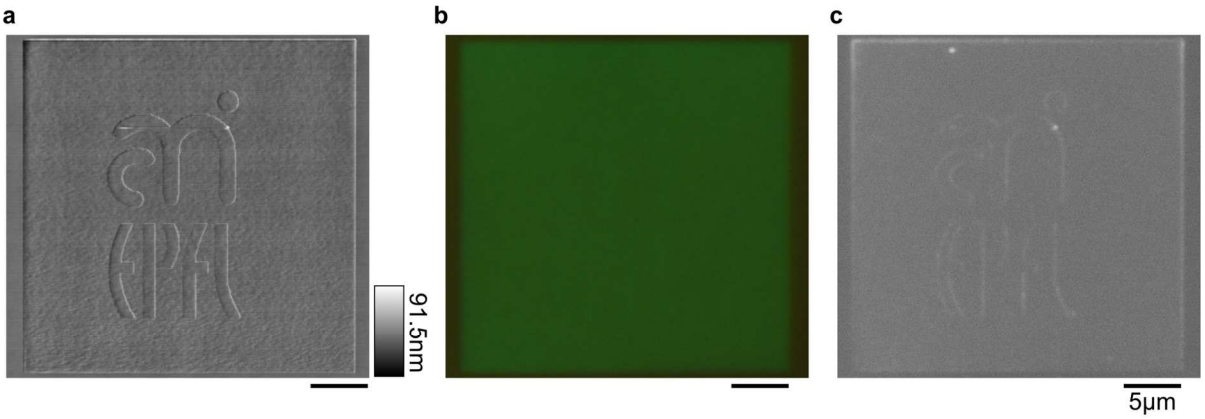

Figure S7. Visibility of 60-90nm deep pattern on a pre-patterned substrate. **(a)** AFM image of a patterned square where in a second scan the AMI/EPFL logo was written. **(b)** Fluorescence image of the same sample where the fluorescence contrast does not allow to see the logos. **(c)** Dark field optical microscopy image where the logos are clearly visible, in particular the rim around the letters gives an optical contrast.

References

(1) Crenshaw, B. R.; Weder, C. Phase Separation of Excimer-Forming Fluorescent Dyes and Amorphous Polymers: A Versatile Mechanism for Sensor Applications. *Adv. Mater.* **2005**, *17* (12), 1471–1476.

(2) Crenshaw, B. R.; Kunzelman, J.; Sing, C. E.; Ander, C.; Weder, C. Threshold Temperature Sensors with Tunable Properties. *Macromol. Chem. Phys.* **2007**, *208* (6), 572–580.

(3) Lott, J.; Ryan, C.; Valle, B.; Johnson, J. R.; Schiraldi, D. A.; Shan, J.; Singer, K. D.; Weder, C. Two-Photon 3D Optical Data Storage via Aggregate Switching of Excimer-Forming Dyes. *Adv. Mater.* **2011**, *23* (21), 2425–2429.

(4) Lavrenova, A.; Balkenende, D. W. R.; Sagara, Y.; Schrettl, S.; Simon, Y. C.; Weder, C. Mechano- and Thermoresponsive Photoluminescent Supramolecular Polymer. *J. Am. Chem. Soc.* **2017**, *139* (12), 4302–4305.

(5) Holzner, F. Thermal Scanning Probe Lithography Using Polyphthalaldehyde. Doctoral Thesis, ETH Zürich, 2013.

(6) Coulembier, O.; Knoll, A.; Pires, D.; Gotsmann, B.; Duerig, U.; Frommer, J.; Miller, R. D.; Dubois, P.; Hedrick, J. L. Probe-Based Nanolithography: Self-Amplified Depolymerization Media for Dry Lithography. *Macromolecules* **2010**, *43* (1), 572–574.

(7) Knoll, A. W.; Pires, D.; Coulembier, O.; Dubois, P.; Hedrick, J. L.; Frommer, J.; Duerig, U. Probe-Based 3-D Nanolithography Using Self-Amplified Depolymerization Polymers. *Adv. Mater.* **2010**, *22* (31), 3361–3365.